processes

MDPI

Article

Collinear Nonlinear Mixed-Frequency Ultrasound with FEM and Experimental Method for Structural Health Prognosis

Hanxin Chen [1,2,*] and Shaoyi Li [1,2]

[1] Nanchang Institute of Science and Technology, School of Artificial Intelligence, Nanchang 330108, China; lisy@ncpu.edu.cn
[2] Wuhan Institute of Technology, School of Mechanical and Electrical Engineering, Wuhan 430074, China
* Correspondence: pg01074075@ntu.edu.sg

Abstract: The principle about the nonlinear ultrasonic mixed frequency is introduced. A novel identification method for incipient structural health prognosis is proposed based on heterolateral co-linear mixed-frequency ultrasound to identify the micro-crack in mechanical structures. The modelling analysis methodology by the application of finite element analysis (FEM) is developed to simulate the nonlinear mixed-frequency ultrasonic wave transmission mechanism from the cracks with different depths and the excited frequency. The correlation models between the crack widths and the mixed-frequency nonlinear coefficients are established. An experimental method based on the nonlinear mixed-frequency ultrasonic theory is proposed to actuate the differential and sum-frequency characteristic mixed waves that interact with the defects of materials, which obtains the nonlinear coefficients to identify the depths of cracks in materials. The FEM model is verified to be effective at predicting the width of the cracks by comparing it with the testing data. The sizes of cracks have a positive correlation with the nonlinear coefficients of the mixed frequencies. A prognosis model for the mixed-frequency nonlinear coefficients is established to predict the crack depths of the specimen.

Keywords: micro-defect identification; collinear mixed frequency; structural health prognosis; nonlinear ultrasound

Citation: Chen, H.; Li, S. Collinear Nonlinear Mixed-Frequency Ultrasound with FEM and Experimental Method for Structural Health Prognosis. *Processes* **2022**, *10*, 656. https://doi.org/10.3390/pr10040656

Academic Editor: Chuanyi Wang

Received: 6 February 2022
Accepted: 14 March 2022
Published: 28 March 2022

1. Introduction

The commonly used material for industrial structures is metal. The critical metal components of the pressure vessels, high-speed wheels and rails, and vehicle components suffer from long-periodic dynamic loads under the harsh and complex extreme working conditions. The fatigue degradation of mechanical components is easily generated, which causes the fracture and failure of the structural materials that bring about the disasters [1–3]. Therefore, the detection of the incipient fatigue cracks in the critical components significantly reduces the probability of the occurrence of these safety accidents. In the industrial field of inspection, the most effective technique for fatigue crack detection is non-destructive testing (NDT). The NDT methods for incipient material damage detection ensure the safety of the industrial systems in service [4].

The nonlinear detection methods, such as second harmonic, can detect the early fatigue cracks in the structural materials [5]. The higher harmonics of the applications in industrial engineering are generated by defects and interspersed by the nonlinearity of the testing system, which makes it much more difficult for the extraction of the target signal. Mixed-frequency ultrasonic detection can make up for the disadvantage of linear ultrasound, which makes the nonlinear mixed-frequency detection method become the hot interest point in the research areas of nondestructive ultrasonic detection (NDT). There are some studies to make contributions to the mixed nonlinear theory and experiments. Jones et al. [6] studied the nonlinear theory about the mixed nonlinear media. The nonlinear fluctuation equations are solved to show the five mixed waves in the medium, which interact with each

other to produce the third column waves. Kalyanasundaram [7,8] proposed the multiscale approach for the mixed nonlinearity of the two isotropic Rayleigh waves and studied the perturbation expansion about the fundamental and second harmonics of the difference frequency components. The nonlinear differential formula is derived by the numerical simulations under the satisfied solvability condition. Walker et al. [9] investigated the relationship between mixed amplitudes and the nonlinear parameters in the identification of the aluminum plate. Lim et al. [10] carried out theoretical and experimental methods for the nonlinear ultrasonic testing of the fatigue cracks. The local nonlinear mechanisms, such as the fatigue cracks, generate the nonlinear harmonics and restrain the linear response such that the amplitudes decrease under the excitation frequency. Chen et al. [11] established the nonlinear Lamb wave detection system to identify the aluminum plates with the different sizes of defects that are generated under the tensile loading cycles. The depths of the defects increase the ultrasonic nonlinear effects of the specimen. Fatigue damage increases the nonlinear response level of the structural materials. The macro-damage of the fatigue fracture has little influence on the nonlinear effect of the structural material. Jiao et al. [12] used an experimental system for collinear mixing frequency measurements. The bispectral analysis of the received mixed waves to analyze the effects of the actuating frequency on the coefficients of the mixed waves was investigated. The method was applicable to detecting and localizing the micro-cracks. Chen et al. [13] studied the analytical solution about the mixed beam to produce the resonant waves. FEA is applied to simulate the two unidirectional mixed nonlinear waves to derive the sufficient conditions for the resonant wave generation during the collinear mixed measurement. The harmonics of ultrasound are applied to diagnose the aluminum plates in the three fatigue plates under the fatigue cycles. The relationship between the nonlinear coefficients and the damage was deduced [14].

The computer-based numerical methods are used as a tool to solve complex structural problems, which are becoming increasingly important. The methods about the numerical analysis were applied to study the propagation mechanism of the guided waves in complex waveguides in various metal structures [15]. Four types of numerical methods are proposed to investigate the propagation and scattering mechanism of ultrasound, which is the finite difference, the finite element, the boundary element, and the semi-analytic finite element [16–18]. The method about finite difference is that the definition domain is dissected into a grid. The differential quotient is replaced by the difference quotient in the fixed solution according to the numerical differentiation formula. The finite element method discretizes the continuous solution into an ensemble of cells. The approximation function in each element piecewise represents the unknown field function in the solution domain. The continuous infinite degree of freedom is changed to the discrete finite degree of freedom. The boundary element method considers the boundary integral equation defined on the boundary as the controlling equation. The boundary element is discretized into the algebraic equations by interpolation. The semi-analytic method combines the analytical and numerical solutions, which improves the computational accuracy and significantly reduces the computational quantity. In engineering applications, the irregular cross-sectional geometry of the acoustic waveguide makes the solution of the propagation of its guided waves difficult to solve by analytical methods. Numerical methods provide a good visual analysis for the theoretical and experimental investigation of guided waves [19]. By setting the relevant parameters of the material, the numerical simulation of the model uses multi-frequency excitation to intuitively select the optimal frequencies and modes for the guided-wave detection. The advantages of numerical methods greatly reduce the experimental cost and bring great economic benefits and guidance for practical industrial measurement [20].

This paper investigates the methodology about the mixed-frequency ultrasound for incipient defect detection. The collinear mixed-frequency ultrasonic detection improves the crack identification accuracy by the amplitudes of the nonlinear ultrasonic components of the sum and difference frequencies. The mixed-frequency nonlinear coefficients of the

experimental data are compared with those of the simulated data to derive the internal relations of the crack sizes with the nonlinear response effects.

2. Mechanism about Collinear Mixed Frequency Ultrasonics

In the experimental method of mixed-frequency ultrasonic testing, two excitation ultrasonic waves with different frequencies are transmitted into the identified specimen synchronously. When no defect is inside the specimen, the two ultrasonic beams adhere to the principle of linear superposition. The two waves do not interfere with each other and interact with the interior micro-structure of materials. The waves propagate with the original constant parameters such as frequencies, wavelength, etc. If defects exist inside the specimen. The defects and ultrasound wave interact to generate the phenomena of the beam superposition with the mixed frequencies that is $\omega_2 \pm \omega_1$. The principle of the heterolateral collinear mixed frequency for nonlinear ultrasonic detection is studied as shown in Figure 1.

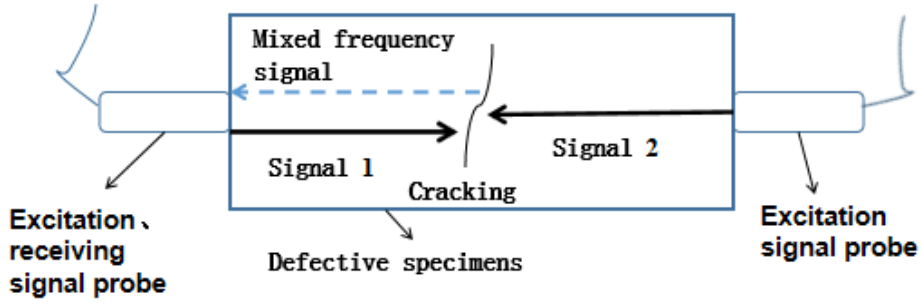

Figure 1. The principle about hetero-side collinear mixing ultrasonic detection.

The nonlinear phenomena occur when ultrasonic waves propagate through the internal defects of materials. The reflected signals from internal defects produce a second harmonic response. When the input ultrasonic waves with multiple frequencies act on the material, the produced nonlinear phenomenon differs from the nonlinear response that the input waves under the single frequency excite. The blend phenomenon at the ultrasound frequencies of the received ultrasonic beams appears. When two excitation signals with different frequencies act on the material synchronously, a complex acoustic field with coupling behaviour emerges inside the material. The complex acoustic field under the coupling condition makes it difficult that the analytic solution of the nonlinear wave formula is accurately obtained. The method for the solution of the nonlinear wave formula does not consider the attenuation factors and ignores the higher-order nonlinear coefficients. The simplified FEA model is established based on the ideal conditions that consider our experimental system and motivation in the research paper [21].

For metallic materials, the attenuation and higher order [22,23] are neglected. The one-dimensional P-wave in the X-direction is considered a sample. The wave path in an isotropic medium is shown in Equation (1).

$$\frac{\partial^2 u(x,t)}{\partial t^2} - c^2 \frac{\partial^2 u(x,t)}{\partial x^2} = c^2 \beta \frac{\partial u(x,t)}{\partial x} \frac{\partial^2 u(x,t)}{\partial x^2} \tag{1}$$

Here, the parameter c is the velocity of the ultrasound, the parameter $u(x,t)$ is the displacement of the particle, and the parameter β is the nonlinear coefficient of the ultrasound. The parameter x is the propagation distance of the ultrasound.

The solution to the wave equation is obtained based on the perturbation theory, which is shown as the following equation:

$$u(x,t) = u^0(x,t) + \beta u^1(x,t) \tag{2}$$

Here, the variable $u^1(x,t)$ is the displacement generated by the material nonlinearity. The variable $u^0(x,t)$ is the linear displacement. When the propagation displacement is proportional to the nonlinear distance, the following equation is obtained:

$$u^1(x,t) = x\omega(\tau) \tag{3}$$

Here $\tau = t - \frac{x}{c}$. The parameter $\omega(\tau)$ is an unknown function.

If the two excitation waves use ultrasound with two different frequencies, the linear displacement is defined as follows:

$$u^0(x,t) = A_1\cos(\omega_1\tau) + A_2\cos(\omega_2\tau) \tag{4}$$

Here, the parameters ω_1 and ω_2 are the frequencies of the two fundamental waves, which satisfy the inequality $\omega_1 < \omega_2$. The parameters A_1 and A_2 are the amplitudes of the two fundamental waves.

The variable $\omega(\tau)$ is defined as follows:

$$\begin{array}{l}\omega(\tau) = -\frac{{A_1}^2{N_1}^2}{8}\cos(2\omega_1\tau) - \frac{{A_2}^2{N_2}^2}{8}\cos(2\omega_2\tau)\\ +\frac{A_1A_2N_1N_2}{4}[\cos(\omega_2-\omega_1)\tau - \cos(\omega_1+\omega_2)\tau]\end{array} \tag{5}$$

Equation (2) is expressed as follows:

$$\begin{array}{l}u(x,t) = A_1\cos(\omega_1\tau) + A_2\cos(\omega_2\tau)\\ +x\beta\left\{\begin{array}{l}-\frac{{A_1}^2{N_1}^2}{8}\cos(2\omega_1\tau) - \frac{{A_2}^2{N_2}^2}{8}\cos(2\omega_2\tau)\\ +\frac{A_1A_2N_1N_2}{4}[\cos(\omega_2-\omega_1)\tau - \cos(\omega_1+\omega_2)\tau]\end{array}\right\}\end{array} \tag{6}$$

Here, the parameters N_1 and N_2 are wave numbers. From Equation (6). The solution to the wave equation includes the frequencies of the excitation signals, which is ω_1, ω_2, second harmonics ($2\omega_1$, $2\omega_2$), sum frequency ($\omega_1+\omega_2$), difference frequency ($\omega_2-\omega_1$). The amplitudes of the waves with the above frequencies are known values. The equation for the nonlinear coefficients (referred to as hybrid nonlinear coefficients) is as follows:

$$\beta = \frac{4}{k_1k_2x}\frac{A_{(\omega_2-\omega_1)}}{A_{(\omega_1)}A_{(\omega_1)}} = \frac{4}{k_1k_2x}\frac{A_{(\omega_1+\omega_2)}}{A_{(\omega_1)}A_{(\omega_1)}} \tag{7}$$

Here, the symbol x represents the propagation distance of the two excitation waves. The symbol $A_{(\omega_1+\omega_2)}$ represents the amplitude of the sum-frequency wave. The symbol $A_{(\omega_2-\omega_1)}$ represents the amplitude of the difference-frequency wave. For the convenience of data processing, the mixed nonlinear coefficients are expressed as follows:

$$\beta^- = \frac{A_{(\omega_2-\omega_1)}}{A_{(\omega_1)}A_{(\omega_1)}} \qquad \beta^+ = \frac{A_{(\omega_1+\omega_2)}}{A_{(\omega_1)}A_{(\omega_1)}} \tag{8}$$

Therefore, the nonlinear coefficients of the difference frequency β^- and the sum-frequency β^+ are inferred and calculated from the parameters of the received waves, which are used to evaluate the damage of the structural material.

3. Ultrasonic Mixed Frequency Testing

3.1. Specimen

The 2A12 aluminum alloy has advantages in specific strength, stiffness, welding properties, stress corrosion resistance, and processing properties. The 2A12 aluminum alloy is widely applied in aircraft, ships, molds, and other fields. The 2A12 aluminum alloy is characterized by its good mechanical and chemical properties and wide applications in industry. The 2A12 aluminum alloy material is used as the testing sample to study the nonlinear mixed ultrasonic technique.

The five samples are cuboids, and their size is 240 mm × 50 mm × 40 mm. The aluminum alloy material specimen is manufactured by wire cutting technology. The triangular notch is prefabricated in the middle of the upper surface of the specimen. The width of the notch is 10 mm, and the height is 15 mm. In order to obtain the plastic zone at the crack tip, the three-point bending test method is used to load the specimen. The three-point bending test is an important experimental method to determine the plastic deformation and bending capability of a metal material. It is widely used in the fields of bending strength, bending modulus, and crack propagation. Compared with the axial tensile testing method, the three-point bending testing method has a special loading mode that makes it more suitable for the prebrication of the plastic zone at the crack tip in the experiment for the nonlinear ultrasonic mixed frequency. The parameters of three-point bending testing are as follows: The fatigue loading force is 10 kN. The three-point bending loading method with a sine wave shape is adopted. The stress ratio is −0.1 and the fatigue loading frequency is 10 Hz.

In the loading experiment, the Instron hydraulic servo universal testing machine with the three-point bending fixture loads the samples. An ultrasonic microscope was used to observe the degradation degree of the samples. The microcracks of different sizes are produced in the opening direction of the prefabricated notch. The $1^{\#}$ sample is non-destructive. The $2^{\#}$–$6^{\#}$ samples have the extended microcrack with the different depths. The defective samples observed by the ultrasonic microscope are shown in Figure 2.

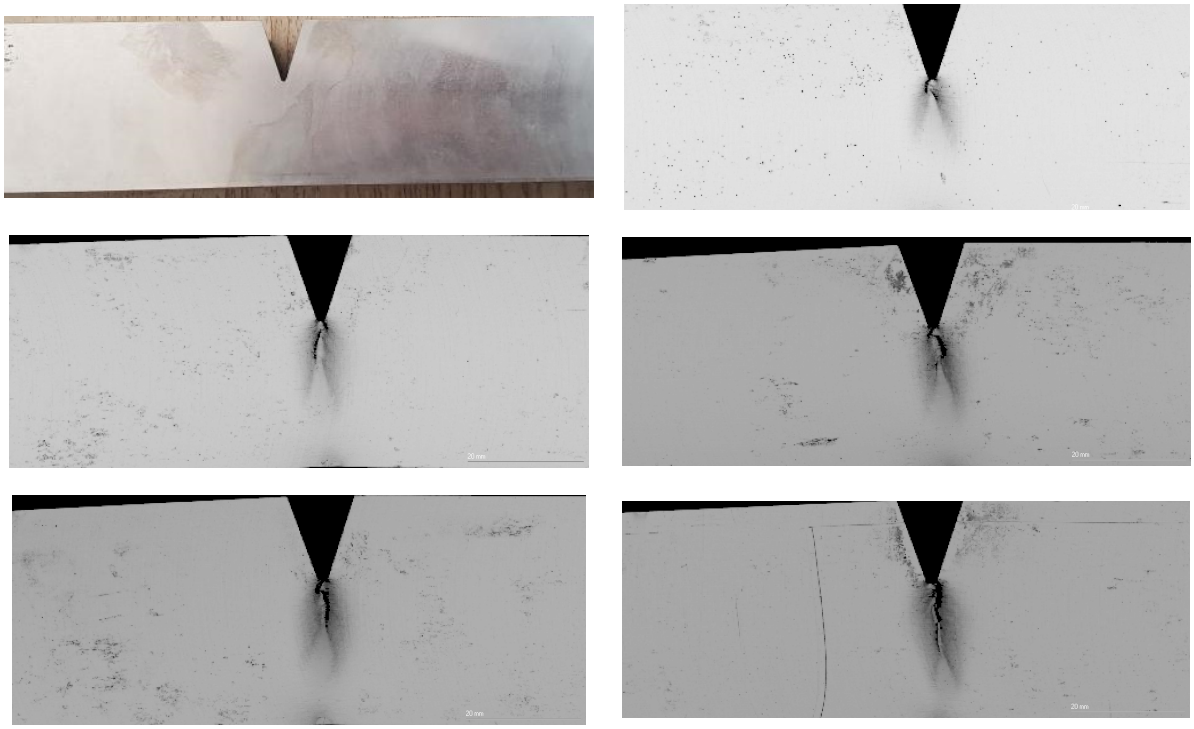

Figure 2. The crack under ultrasonic microscope.

3.2. Experimental Setup

The excitation and receiving systems for the nonlinear ultrasonic detection method are designed, which is based on the theory about the collinear anisotropic mixed-frequency ultrasound. Figure 3 shows the theory about the nonlinear collinear experimental system. Figure 4 shows the experimental platform. The experimental platform mainly consists of the nonlinear high-energy ultrasonic system RAM-5000 SINAP, a broadband transducer, a narrowband longitudinal transducer, an RDX-6 diplexer, a shear wave transducer, and an oscilloscope. The type of ultrasonic microscope is the ultrasonic scanning microscope SAM300, with a maximum penetration depth of 15 mm and an optimal theoretical res-

olution of 12 μm. The bit resolution of the ultrasonic signal is 256 bits. The sampling frequency is 14 MHz. The chosen window function of the fast Fourier transform (FFT) is the Hanning window. The trigger signal is sent from the computer. RAM-5000 SINAP is a signal generator. The first channel of RAM-5000-SNAP is connected to the broadband transducer. The second channel of RAM-5000-SNAP is connected to the narrowband longitudinal wave transducer. The RDX-6 duplexer is connected to the shear wave transducer to make the shear wave transducer act as both the transmitter and receiver. The beam of two ultrasonic waves with different frequencies interacts with the defect inside the specimen to stimulate the nonlinear response of the local micro-structure of the internal material. The mixed-frequency ultrasonic wave is acquired by the shear wave transducer and transmitted via the duplexer to first channel of the RITEC SNAP RAM-5000.

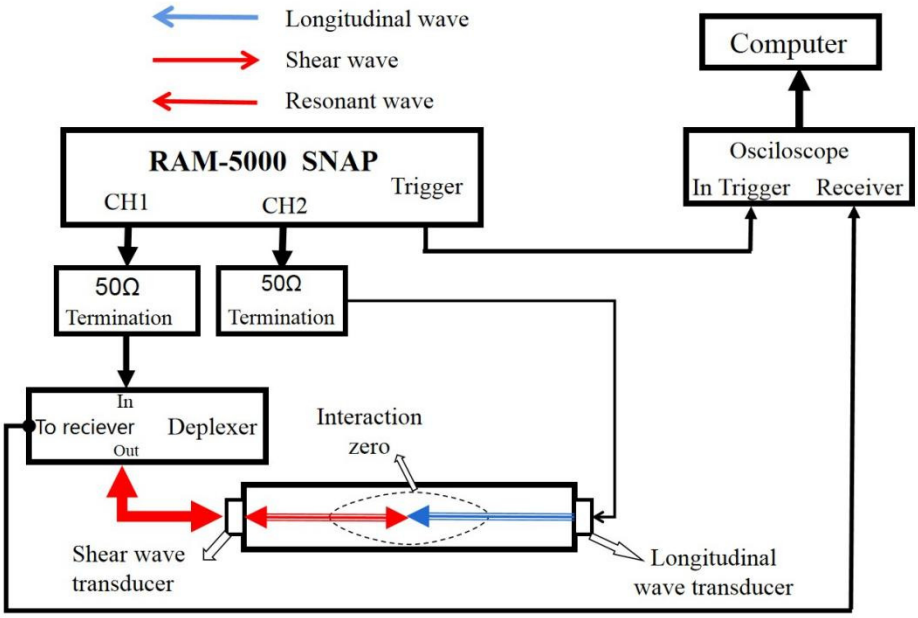

Figure 3. The theory about an experimental system.

Figure 4. Experimental platform.

The detection of metal fatigue damage with the nonlinear ultrasonic mixed technique needs to effectively avoid the nonlinear signal interference from the nonlinear testing system, which obtains the much more accurate nonlinear signal related to the damaged

structure [5]. The experimental optimal nonlinear response wave is determined by the adjusting parameters of the mixed frequency waves. The interaction of the two ultrasonic waves with the crack is generated in the process of wave transmission with weak characteristic energy. The experimental method depends on adjusting the parameters of the nonlinear ultrasonic system to obtain the optimal nonlinear response of the mixed frequency waves from the crack. The optimal excitation frequency in the experimental process enhances the obvious mixed-frequency waves, which are shown in the microscope. Based on industrial experience with the above analysis, we chose the 2.25 MHz and 5 MHz transducers as excitation and receive sensors. The 5 MHz transducer acts on two actions. The first function is to inject the incidence signal, and the second function is as the reception of the output signal by using the duplexer. The frequency response curves of the two transducers are shown in Figure 5. Actually, the experimental frequencies of the incidence signals are set to be 1.8 MHz and 4.6 MHz. The reason is as follows: (1) The frequency difference is 2.8 MHz between the two columns of ultrasound, which is large enough to be easily distinguished during spectral analysis. (2) The second-order harmonics are 3.6 MHz and 9.2 MHz. The sum-frequency signal is 6.4 MHz, which is quite different and does not affect each other.

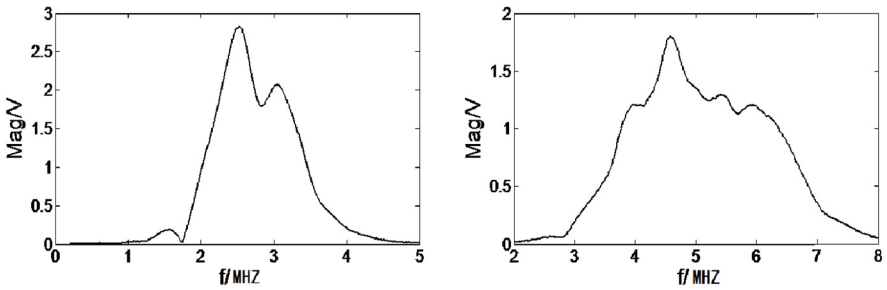

(**a**) (**b**)

Figure 5. Frequency response (**a**) 2.25 MHz transducer, (**b**) 5 MHz transducer.

4. FEA for Fatigue Damage

4.1. FEA Model

The used aluminum alloy specimen in the FEA model for numerical simulation is rectangular. The size of the specimen is 24 mm × 4 mm × 5 mm. The triangular notch in the middle is 1 mm wide at the bottom and 1.5 mm high. One 3D solid model is established in the ABAQUS part module as shown in Figure 6.

The stress-strain curve for the intrinsic structural relationship of 2A12 aluminum alloy is obtained by conducting tensile testing on the material. The length of the specimen is 150 mm. The length of the tensile zone is 60 mm. The diameter is 10 mm, as shown in Figure 7.

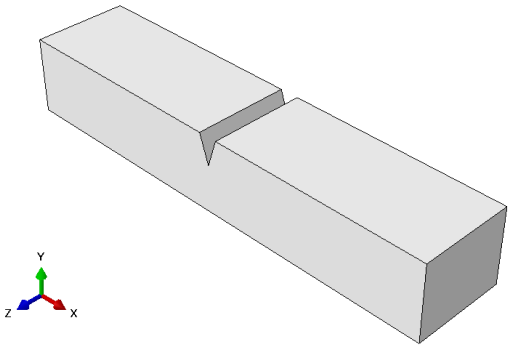

Figure 6. Finite element model of aluminum alloy specimen.

Figure 7. 2A12 aluminum alloy tensile specimen.

4.2. Material Properties

The tensile testing experimental system adopts the MTS microcomputer-controlled electronic universal tensile test machine. The loading rate is 0.8 mm/s. The mechanical properties of the steel wire are little affected by temperature. It is necessary to conduct the tensile testing of the steel wire at room temperature. The tensile rate is 1 mm/min. When the testing piece breaks, the testing ends. The stress concentration occurs in the middle of the specimen. The tensile data is collected for measurement.

The engineering stress σ_e and engineering strain ε_e obtained from the testing data are transformed into the true stress σ_T and true strain ε_T. The derivation process is as follows: the symbol l_0 is the axial length of the specimen before stretching. The symbol l_I is the axial length of the specimen after stretching. The engineering strain is defined as follows:

$$\varepsilon_e = \frac{l_1 - l_0}{l_0} \tag{9}$$

The true response ε_T becomes.

$$\varepsilon_T = \int_{l_0}^{l_1} d\varepsilon_T = \int_{l_0}^{l_1} \frac{dl}{l} = \ln \frac{l_1}{l_0} = \ln(1 + \varepsilon_e) \tag{10}$$

It is assumed that the volume of the specimen is constant during the stretching process. The following equation is derived:

$$l_0 S_0 = l_1 S_1 \tag{11}$$

Here, S_0 is the cross-sectional area of the specimen before deformation, S_1 is the cross-sectional area of the specimen after deformation.

The true stress σ_T is defined as follows:

$$\sigma_T = \frac{F}{S_1} = \frac{F}{S_0}(1 + \varepsilon_e) = \sigma_e(1 + \varepsilon_e) \tag{12}$$

To ensure the accuracy of the tensile experimental data, three specimens were tested for stress tension. The three groups of stress-strain data are collected, which is transformed into the real stress-strain by Equations (10) and (12). The fitting curve is the average values as shown in Figure 8.

The initial modulus is defined as follows:

$$E_0 = \frac{\sigma_2 - \sigma_1}{\varepsilon_2 - \varepsilon_1} \tag{13}$$

Here, $\varepsilon_1 = 0.00025$, $\varepsilon_2 = 0.0005$, the stress (σ_1) is corresponding values of the strain (ε_1). The stress (σ_2) are the corresponding values of strain (ε_2). The initial modulus of the 2A12 aluminum alloy is 20,060.58 MPa.

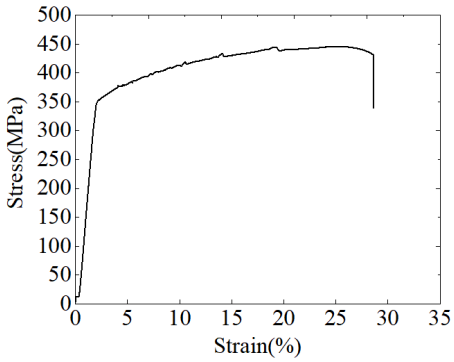

Figure 8. Real stress-strain curve.

The overall actual strain of the material includes both elastic and plastic strains. The elastic strain is separated from the plastic strain, i.e., the elastic strain is subtracted from the overall strain to obtain the plastic strain [24]. The equation about the relationship between the actual plastic strain and the actual elastic strain is shown as follows:

$$\varepsilon_{pl} = \varepsilon_l - \varepsilon_{el} = \varepsilon_l - \frac{\sigma}{E} \tag{14}$$

Here, the variable ε_{pl} is the actual plastic strain, the variable ε_{el} is the actual elastic strain, the variable ε_l is the overall actual strain, the parameter E is the modulus of elasticity, and the variable σ is the actual stress.

Table 1 shows the experimental data that is used as the input values into the ABAQUS finite element simulation and converted to plasticity settings, which are collected from the experimental stress-strain actual measurements on the specimen.

Table 1. Experimental data and input parameters for ABAQUS plasticity setup.

Experimental Data		ABAQUS Input Data		
Nominal Stress (MPa)	**Nominal Strain**	**Actual Stress (MPa)**	**Actual Strain**	**Plastic Strain**
354.0771905	0.002673568	355.0238398	0.00267	0
354.1087495	0.002683295	355.0589276	0.002679701	9.70×10^{-6}
354.163946	0.002693293	355.1178134	0.002689673	1.97×10^{-5}
354.2112464	0.002703292	355.1687829	0.002699645	2.96×10^{-5}
354.24278	0.002713291	355.2039438	0.002709617	3.96×10^{-5}
354.2979766	0.002723018	355.2627364	0.002719317	4.93×10^{-5}
354.3453024	0.002732747	355.3136386	0.00272902	5.90×10^{-5}
354.376836	0.002742475	355.3487054	0.002738721	6.87×10^{-5}
354.4083696	0.002752202	355.3837729	0.002748421	7.84×10^{-5}
354.4556953	0.0027622	355.434773	0.002758393	8.84×10^{-5}
354.5029958	0.00277193	355.4856532	0.002768095	9.81×10^{-5}
354.5266588	0.002781657	355.5128302	0.002777795	0.000107795
354.5581925	0.002791114	355.5478048	0.002787226	0.000117226
354.6054927	0.002800844	355.5986874	0.002796929	0.000126929
...	...	...	...	...

4.3. Parameter Set in FEA

4.3.1. Time Step

The simulation procedure of the ultrasonic propagation under loading conditions includes the static general analysis step and the dynamic explicit analysis. The former corresponds to the load analysis. The latter corresponds to the ultrasonic propagation simulation. The difficult point in the loading analysis is the nonlinear convergence. Here, dynamic explicit analysis is used in the simulation of ultrasound, and there is no problem

with convergence. Generally, only the timing of steps is set according to the length of the process.

The main factor that affects the calculation accuracy in FEA is the integration time step (Δt). The smaller values for the step time (Δt) cause the calculation to be more accurate. The Newmark time integration method is used, which make it reasonable to take $\Delta t = \frac{1}{f_m}$ for time step (Δt). Here the parameter f_m is the highest frequency of the ultrasonic propagation wave.

4.3.2. Loading Boundary Condition

The numerical simulation of the propagation mechanism of the mixed frequency guided waves in aluminum alloy by FEA is actually about the propagation of the excited vibration mode along the angle steel. The two sets (set-1, set-2) are exerted at both ends, which consist of the different frequency excitation waves or displacement loads. The FEM model for aluminum alloy uses the force to stimulate the actual vibration, which is exerted at the end of the set. The boundary conditions are fully fixed constraints on the eight vertices of the aluminum alloy, as shown in Figure 9.

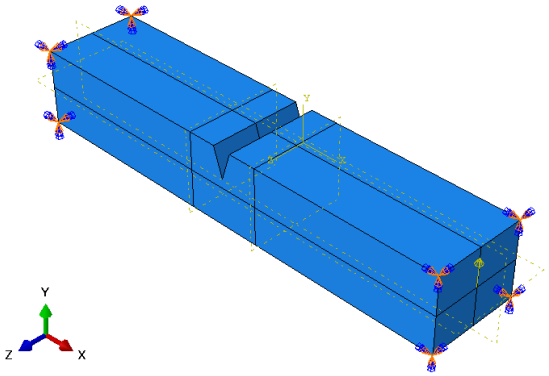

Figure 9. Boundary condition of FEM model.

4.3.3. Cell Size

In the numerical simulation of the ultrasonic wave propagation in composite laminates, the dynamic explicit analysis in the kinetic equations is used to ensure stability. The maximum size of the grid elements in the numerical simulation model is calculated based on the wavelength of the ultrasonic waves. More than 10 grid elements within one wavelength of the ultrasonic wave are satisfied to make the wave propagation to obtain a much more accurate simulation. Because of the property of the dispersion and the multi-mode phenomenon in the ultrasonic wave propagation within the composite material, the condition is satisfied by the following equation:

$$l_e \leq \frac{\lambda_{min}}{10} \tag{15}$$

Here, the parameter l_e is the element size, the parameter λ_{min} is the minimum wavelength. The minimum transverse velocity of the mixed-frequency ultrasound is 3100 m/s. The maximum value of the frequency component is 300 kHz.

$$f_{max} = 300 \text{ kHz} = 3 \times 10^5 \text{ s}^{-1} \tag{16}$$

$$\lambda_{min} = \frac{C_T}{f_{max}} = \frac{3100 \text{ m/s}}{3 \times 10^5 \text{ s}^{-1}} = 10.3 \text{ mm} \tag{17}$$

$$l_e \leq \frac{\lambda_{min}}{10} = 1.03 \text{ mm} \tag{18}$$

The size of grid element is 0.5 mm to ensure that 10 grids are included in one wavelength with much better resolution, as shown in Figure 10.

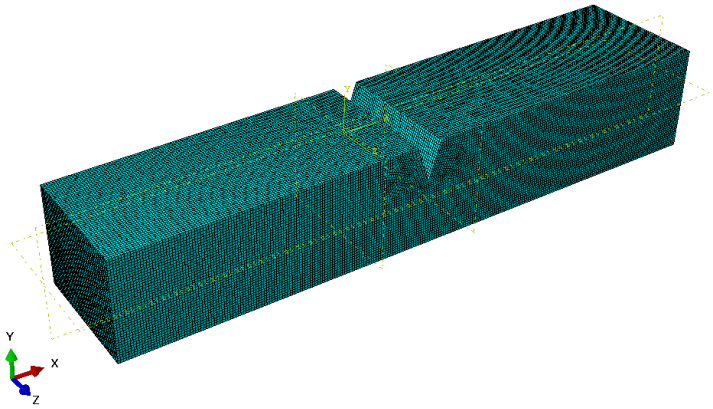

Figure 10. Meshing of the FEA model.

5. Simulation on Effect of Damage Growth on Nonlinear Response

5.1. Effect of Crack Depth on Nonlinear Coefficients

The effect of different crack depths on the nonlinear coefficients is investigated. Multiple sets of numerical simulations are conducted. The crack depth is variable, and the other parameters are consistent. The constant crack width is 100 μm, and the crack length is varied for the numerical simulation. The crack lengths were 0 mm, 0.41 mm, 0.6918 mm, 0.7624 mm, 0.805 mm, and 1.2215 mm. Figure 11 shows the positions of the incidence waves that are exerted at both ends with the frequencies (180 KHz, 460 KHz) and the received mixed frequency signals.

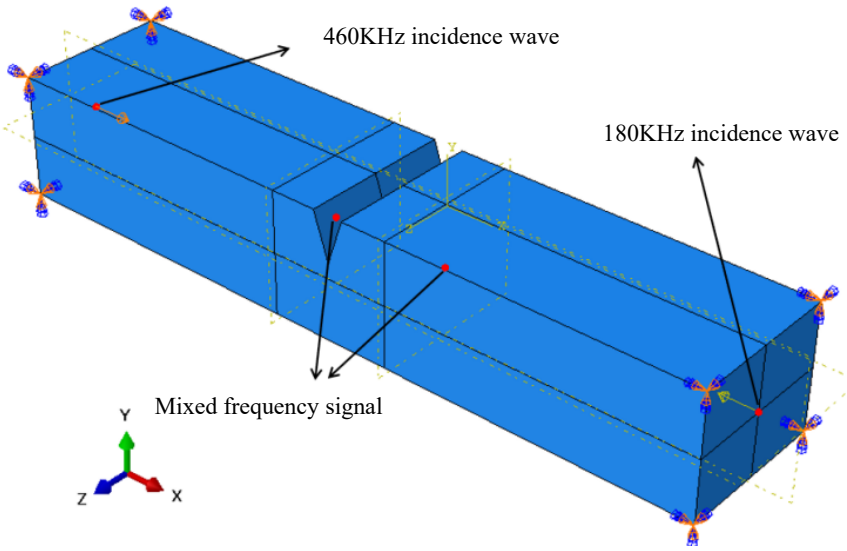

Figure 11. Excited incidence waves and received signal in the FEA model.

As described in Section 4.1, the size of the FEA model is 24 mm × 4 mm × 5 mm. In an FEA model, we can obtain the simulated signal based on what we require. Here we choose the location of the received mixed-frequency signal at x = 15 mm. The echo signal is acquired for the cracks at the different depths. The spectral analysis is obtained after the fast Fourier transform (FFT). Figure 11 shows the simulated signal and spectrum. The nonlinear spectrum of the received mixed frequency signals contains the two fundamental frequency components. The two ultrasonic waves excited the material crack to generate a

nonlinear response, which consists of the sum-frequency component and the differential frequency component.

In the process of mixed waves passing through micro-cracks, there is a "breathing effect" at the micro-cracks suffered from the periodic tensile/compressive action of the ultrasound, which is the cause of the nonlinear response phenomena [6–8]. The sum frequency, difference frequency, and multiplication frequency components are observed in the spectrum of the received mixed frequency waves. From the magnitudes of the sum and difference frequency components shown in Figure 12, the values of the nonlinear coefficients for the crack depths are calculated based on Equation (8), which is shown in Table 2.

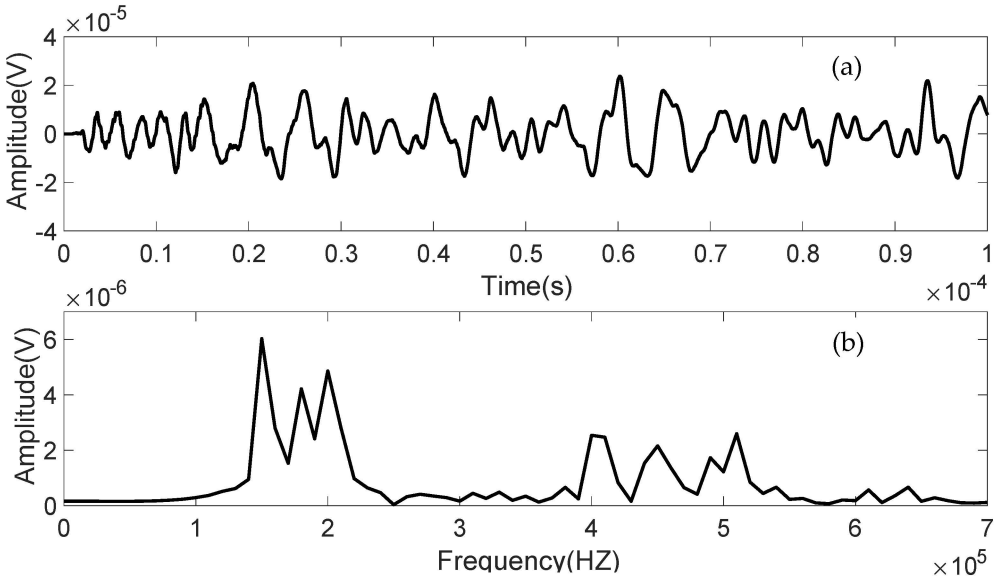

Figure 12. (**a**) Simulated signal (**b**) spectrum.

Table 2. Nonlinear coefficients at different crack depths.

Crack Depth/mm	Differential Frequency Nonlinearity Coefficient β^- (10^4)	Sum Frequency Nonlinearity Coefficient β^+ (10^4)	Relative Coefficient of Mixing Frequency Nonlinearity $\hat{\beta}$ (10^4)
0	1.879	4.851	6.73
0.41	2.384	5.791	8.175
0.6918	3.729	7.249	10.978
0.7624	4.564	7.989	12.553
0.8505	6.263	9.713	15.976
1.2215	10.705	18.696	29.401

Figure 13 shows the trend of the nonlinear factors with crack depth. In Figure 14, the fitted curve equation for the difference frequency is $H^- = 7.66202\beta^{-2} - 2.04331\beta^- + 1.86397$. The value of the complex correlation coefficient factor R^2 equals 0.98232. In Figure 15, the fitting curve equation of the sum-frequency is $H^+ = 14.23083\beta^{+2} - 6.48113\beta^+ + 5.13304$ and the value of the complex correlation coefficient factor R^2 equals 0.9827. In Figure 16, the fitted curve equation for mixed frequency is $H^+ = 21.89284\beta^{+2} - 8.52443\beta^+ + 6.99701$ and the value of the complex correlation factor R^2 equals 0.98996.

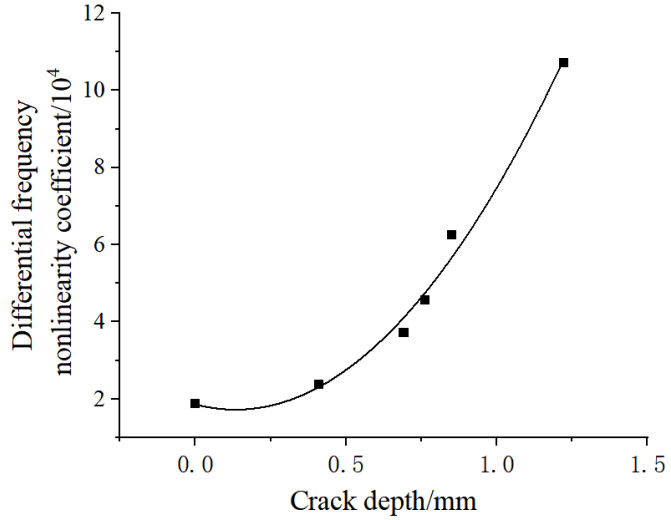

Figure 13. Relation between differential frequency and crack depth.

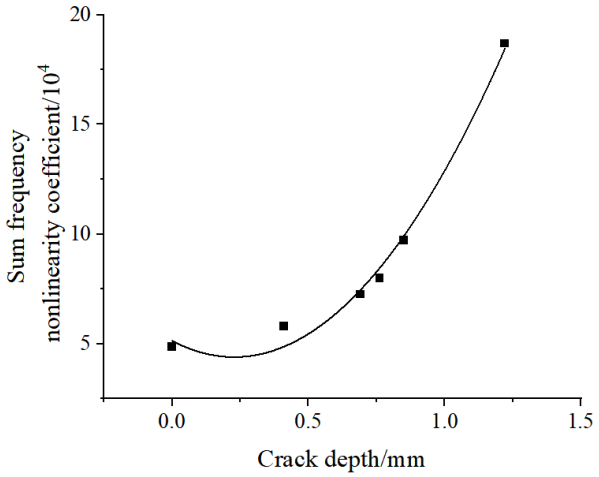

Figure 14. Relation between sum frequency and crack depth.

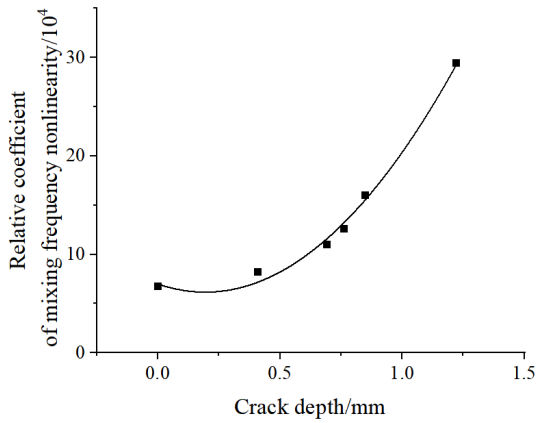

Figure 15. Relation between mixed-frequency factor and crack width.

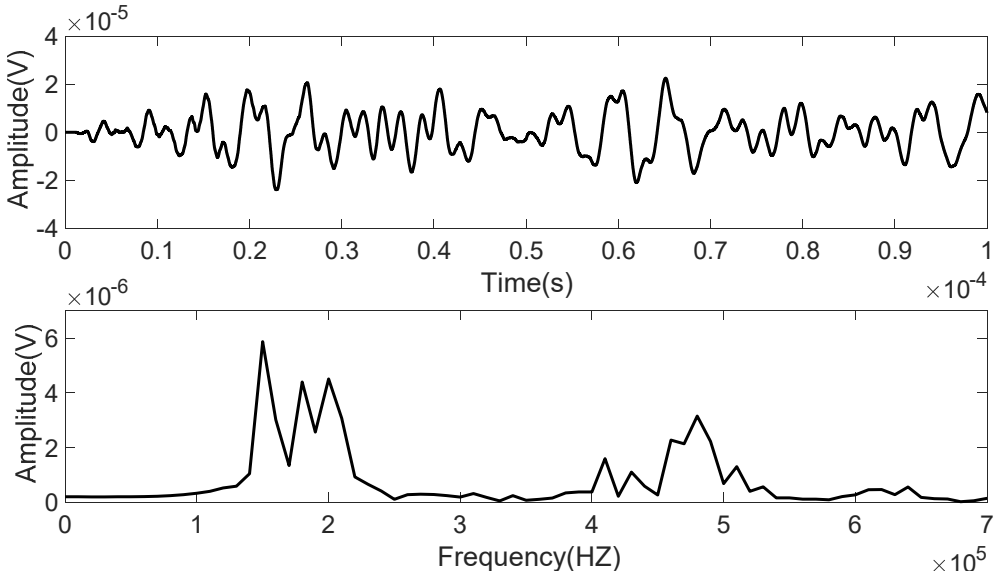

Figure 16. Simulated signal spectrum at different crack widths.

In Table 2, the nonlinear response is correlated with the crack growth. The nonlinear coefficients β^-, β^+, and $\hat{\beta}$ are positively correlated with the crack length within a certain range. The nonlinear coefficients are sensitive to the microcrack growth with nonlinearity. The vibrations generated by the mixed-frequency ultrasonic waves passing through the microcrack create the pull/pressure effect on both sides of the microcrack interface. The microcrack produces a pull/pressure effect to make point contact tend to occur between the interfaces under the action of ultrasonic waves. The displacement generated by ultrasonic waves at the microcrack becomes larger, which produces the relatively concentrated stress with the larger values at the concentration point. The distortion of the ultrasonic waves, to a certain extent, occurs. The contact area of the two sides of the microcrack increases the tensile/compression effect and the nonlinear contact response becomes stronger. The nonlinear phenomenon becomes more obvious to increase the nonlinear coefficients.

5.2. Effect of Crack Width on Nonlinear Coefficient

Previous investigations show that the depth of cracks in the material in the free condition has a significant effect on the property of ultrasonic propagation. There are fewer research results about the effect of crack width on nonlinear ultrasonic response excited by mixed frequencies. The damage growth along the width direction is not avoided. It is necessary to explore the effect of crack width on the nonlinear ultrasonic wave propagation behavior at mixed frequencies. The FEA model used in the paper has a constant 300 μm deep crack that is 20 μm, 40 μm, 60 μm, 80 μm, and 100 μm wide. Based on the discussion in Section 4, FEA models containing defects with different widths are constructed. The metal structure with the crack sizes of an interval of 20 μm width is used as samples to explore the effects of the microcracks of the different widths on the nonlinear coefficients, which are exerted by the loading of mixed frequency ultrasonic waves.

The echo signals were obtained at $x = 15$ mm with the different crack widths. The spectral analysis was obtained by FFT, as shown in Figure 16. The nonlinear coefficient β is calculated by the derived equation as shown in Equations (7) and (8). The nonlinear relationship between the nonlinear coefficients and the microcrack widths under the effect of the mixed frequency ultrasonic waves is summarized in Figures 17–19. It is demonstrated that the nonlinear coefficients show a descending trend with ascending crack widths.

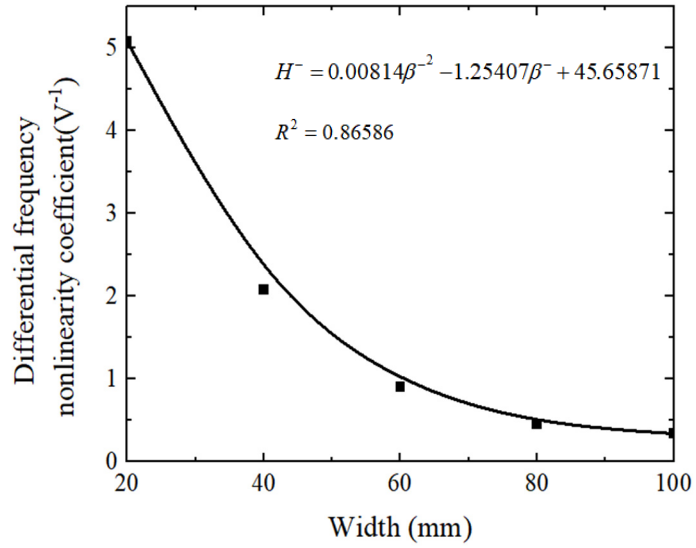

Figure 17. Variation of differential frequency factor with crack width.

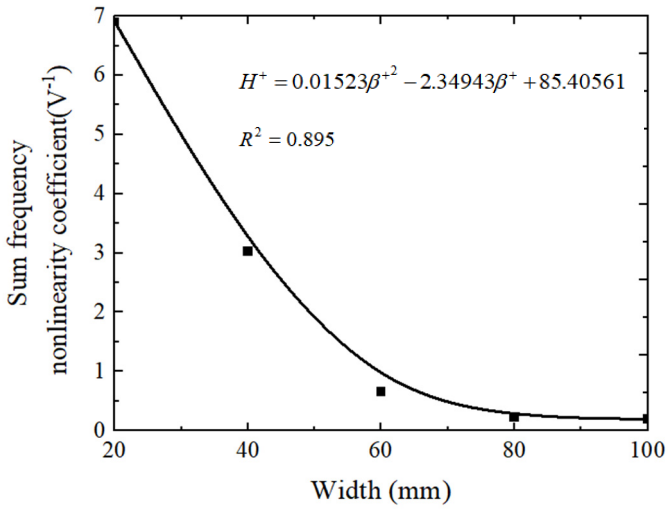

Figure 18. Variation of sum frequency factor with crack width.

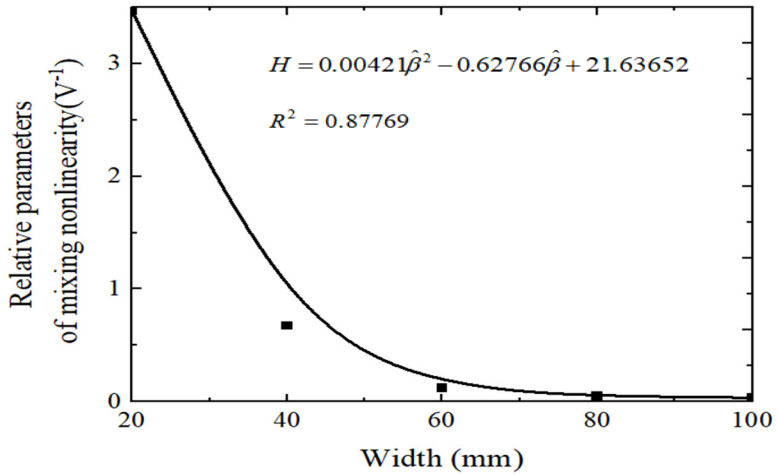

Figure 19. Variation of mixed frequency factor with crack width.

When the ultrasonic wave propagates in the elastic medium in its free state, the particle vibrates in the longitudinal and transverse directions. The transverse vibration excitation causes the interface of the crack to generate the slap effect, and the longitudinal vibration excitation causes the crack to generate the slip effect, which gives rise to the periodic opening and closing of the crack interface. When the transverse displacement amplitude is greater than the crack opening width, which makes the crack interface close under the effect of the transverse vibration compressive stress, the sound waves continue to transmit through the cracked medium. If the crack is not closed and no stress transfer exists under the nonlinear excitation, the crack surface gives rise to the harmonic components of the nonlinear wave, which come from the nonlinear response of the vibration of the crack interface. With the increased expansion of microcracks, the periodic opening and closing effect decreases, which attenuates the nonlinear response engendered by the flapping and sliding of the crack interface. When the two mixed-frequency waves interact with the interface of the microcrack, the crack of the mechanical component becomes wider, which weakens the effect of the transverse vibration and reduces the nonlinear effect. On the contrary, it enhances the nonlinear effect of the local structure of the crack material.

Nonlinear mixed-frequency ultrasound is different from the traditional linear ultrasonic testing. In the single linear ultrasonic detection of defects, the reflection and refraction of ultrasound waves pass through the defects, which is characteristic of the transform of amplitudes or phases of acquired echo signals after waveform conversion. The larger the defect in the tested specimen produces, the more obvious the reflection, refraction, or waveform conversion of the ultrasonic wave, which makes the defect easier to detect. The nonlinear detection is contrary to the generation mechanism of linear ultrasound. The larger width of the defect makes it much more difficult to detect.

6. Prognosis for Fatigue Growth with Experimental Data Analysis

6.1. Experimental Data Analysis

The frequencies of the two excitation signals $1^{\#}$ and $2^{\#}$ were set to be 1.8 MHz and 4.6 MHz. The response of the transducers is shown in Figure 20. The two columns of the ultrasonic waves were used to conduct the experimental nonlinear collision of the mixed frequency ultrasound on the fatigue cracks with the different crack depths as discussed in Section 3. Figure 21 shows the spectrum of the acquired mixed-frequency signals from the $6^{\#}$ sample.

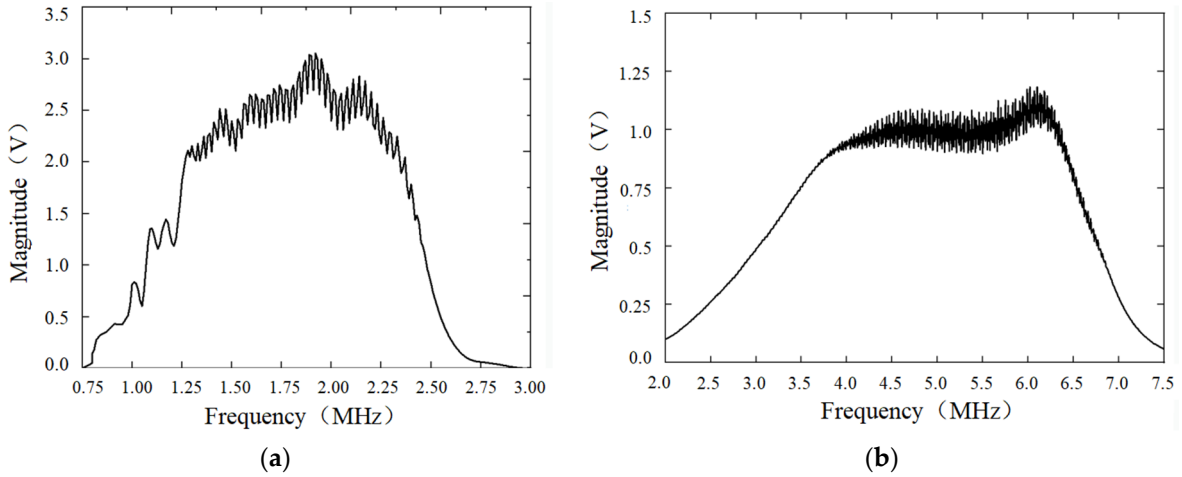

Figure 20. Spectrum of transducers with center frequencies (**a**) 1.8 MHz, (**b**) 4.6 MHz.

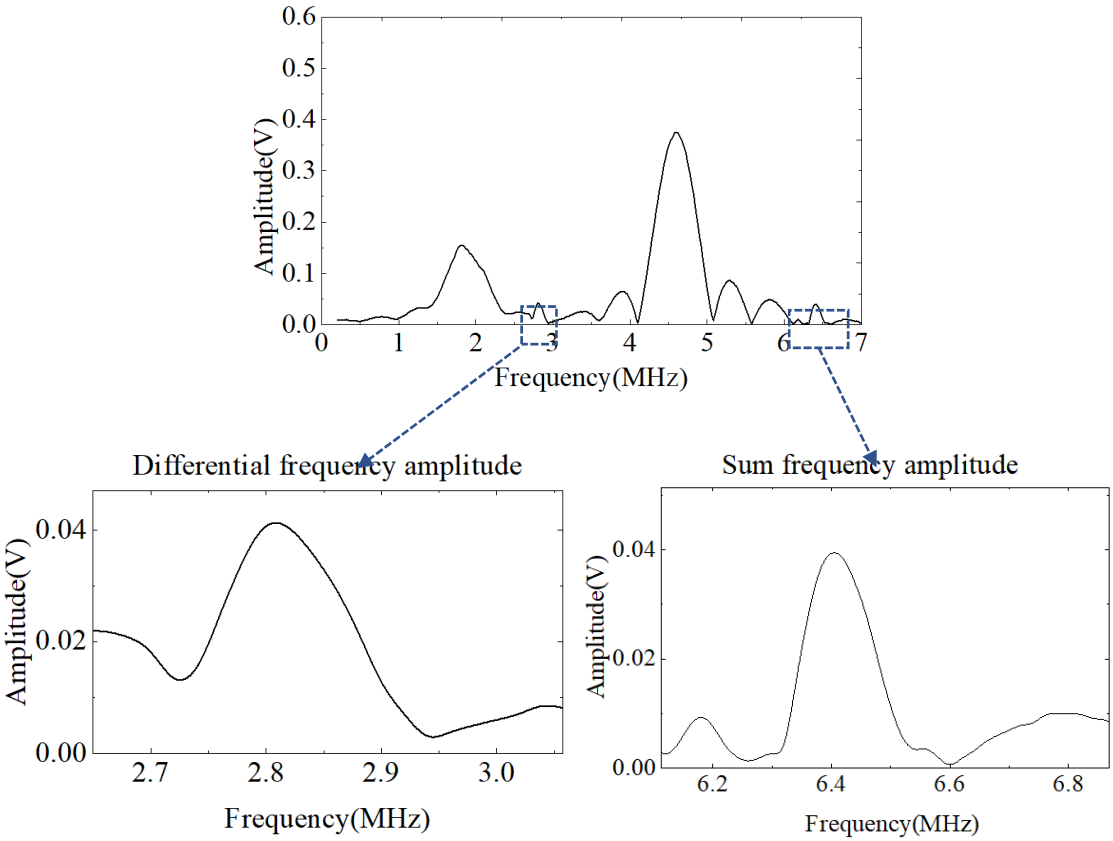

Figure 21. $6^{\#}$ specimen received signal spectrum diagram.

As demonstrated in Figure 21, the frequency components in the spectrogram of the acquired mixed-frequency signals are complex. The fundamental signal has different characteristics with the amplitudes of the differential frequency (2.8 MHz) and the sum frequency (6.4 MHz).

The amplitudes of the difference frequency signal $(A_{(\omega_1-\omega_2)})$ is 0.042 V and the amplitudes of the sum frequency signal $(A_{(\omega_1-\omega_2)})$ is 0.04 V. The inequality of the amplitudes between the difference frequency and the sum frequency is due to the attenuation in the process of ultrasonic propagation, which is related to the frequencies of the component signals. The attenuation of the amplitudes of the two mixed-frequency signals is not the same. The amplitudes of the difference frequency signal and the sum frequency signal are not exactly the same.

The sum frequency nonlinearity coefficient β^+ and the differential frequency nonlinearity coefficient β^- are calculated by the collected mixed frequency ultrasonic signals from the samples with different crack depths, which are shown in Table 3. The experimental mixed-frequency signals are repeated three times for one specimen to calculate the average values, which is used to reduce the error of the nonlinear coefficients.

Table 3. Nonlinear coefficient for crack depth.

Item \ Sample	$2^{\#}$	$1^{\#}$	$3^{\#}$	$5^{\#}$	$6^{\#}$
Crack depth (mm)	4.1	6.918	7.624	8.505	12.215
Differential frequency (β^-)	0.2335	0.2632	0.3440	0.3506	0.7226
Sum frequency (β^-)	0.2179	0.2723	0.3796	0.4308	0.6882

As demonstrated in Table 3 and Figure 22, the difference frequency nonlinear coefficient β^- and sum frequency nonlinear coefficient β^+ increase monotonically with the ascending trend of the fatigue damage growth, which shows that the nonlinear coefficient is positively correlated with the crack depth. The intrinsic physical generation mechanism is that the contact area of the crack interface increases. The nonlinear effect becomes more and more obvious.

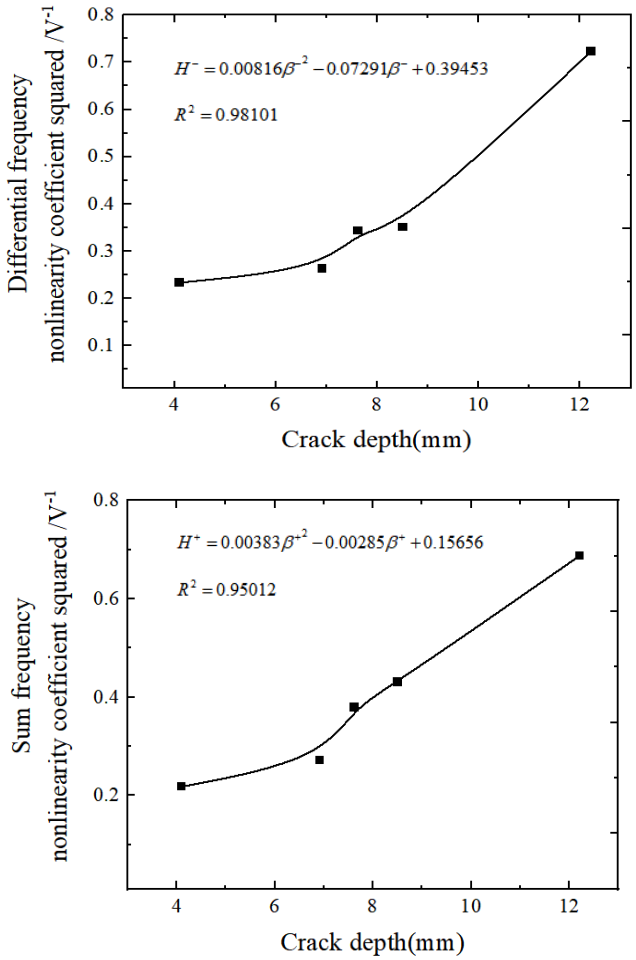

Figure 22. Nonlinear coefficient versus crack depth.

6.2. Prediction of Fatigue Crack Depth

In collinear mixed-frequency ultrasonic testing, the mixed-frequency nonlinear coefficient is closely related to the micro-structure of metal materials under different fatigue cycles. The crack depth of the specimen affects the nonlinear effect of the ultrasonic wave. The mixed frequency nonlinear coefficients effectively evaluate the crack depth of materials. This relationship provides the basis for the prediction of crack growth of metal specimens under rising fatigue cycles.

The experimental data approximation is shown in Table 3 and the corresponding equation between the crack depth H and the nonlinear coefficients (β^-, β^+) is derived as follows:

$$H = -46.17\beta^{-2} + 59.28\beta^- - 6.53 \quad (19)$$

$$H = -16.67018\beta^{+2} + 3.104273\beta^+ - 1.2922 \quad (20)$$

The correlation between the fitted equation and the actual value is characterized by the complex correlation coefficient (R). The correlation coefficient is much closer to one and the equation fits better. The inequality $R > 0.8$ indicates that the fitting curve and the equation have an extremely strong correlation. Here, the complex correlation coefficients R

of the nonlinear coefficients β^-, β^+ are 0.93337 and 0.9126. The two fitted equations have good fitting accuracy.

According to the fitting curve between the mixed frequency nonlinear coefficients and the crack depth of the specimen, there is an approximate quadratic fitting relationship between the mixing nonlinear coefficient and the crack depth. The fitting curve is verified to be used as the prognosis model to predict the crack growth of the metal specimens based on the collinear mixed frequency testing technology.

The difference frequency nonlinear coefficient and the sum frequency nonlinear coefficient are effective for predicting the crack depths of the specimen. In order to emphasize the relationship between the mixed frequency nonlinear coefficients and specimen crack depth, the relative characteristic parameters of the mixed nonlinear are proposed to predict the crack growth based on the data fusion theory. The difference frequency nonlinear coefficients and sum frequency nonlinear coefficients are directly proportional to the difference frequency/sum frequency signal amplitudes of the received ultrasonic signal. The nonlinear mixed frequency synthesis parameter is defined as $\hat{\beta} = \beta^- \times \beta^+$.

As shown in Table 3 of the experimental data, the equation of the fitted curve between the crack depth H of the specimen and the mixed frequency nonlinear relative parameter $\hat{\beta}$ is as follows:

$$H = -57.77028\hat{\beta}^2 + 47.9898\hat{\beta} + 2.62737 \quad (21)$$

Because the fitted complex correlation coefficient R is equal to 0.87966. The fitted curve equation reflects the relationship between the nonlinear relative parameters of mixed frequency and the crack depth of the specimen. The relationship is shown in Figure 23.

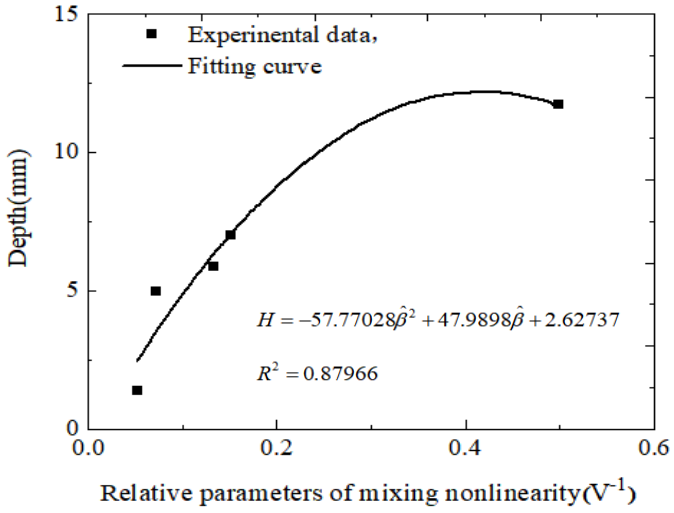

Figure 23. Relationship between nonlinear mixing relative parameters and crack depth.

The relative parameters of the mixed nonlinearity, sum-frequency nonlinearity coefficients, and differential-frequency nonlinearity coefficients were calculated for the specimens at different crack depths. The relationship between the nonlinear coefficients β^-, β^+ and $\hat{\beta}$, and the crack depths of the specimens were predicted, and the results are shown in Figure 20.

The fitting functions and the coefficient R^2 are derived based on data fitting, which has definite values. The data are the average values, which are obtained by repeating experiments multiple times. The average values of the experimental data reduce the uncertainty of the experiment and calculate the measurement error.

As shown in Figure 24, the above fitted curve equation can well characterize the relationship between the nonlinear coefficients and the crack depth of a specimen based on the analysis of the average error of the crack depth prediction by using the difference frequency, sum frequency, and mixing nonlinear relative coefficient. The average error of prediction based on the mixed frequency nonlinear relative coefficients is the smallest. The prediction

model based on the relative parameters of the mixed frequency nonlinearity fully shows the dependence between the crack depth and the mixed frequency nonlinearity coefficient.

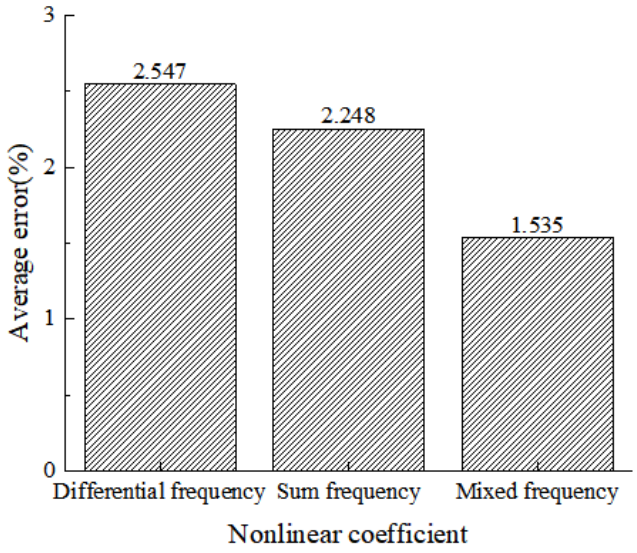

Figure 24. Prediction of crack depth by the nonlinear coefficient.

7. Conclusions

It is verified that the values of the nonlinear coefficients increase with the ascending crack depth within a certain range. The numerical simulation results are highly consistent with the experimental data. The nonlinear mixed-frequency ultrasonic simulation model is feasible and effective. The effective models about the collinear mixed-frequency ultrasonic simulation with the different crack widths are established. Under the exerting action of the mixed-frequency ultrasound, the pattern of the descending nonlinear coefficients with the ascending crack width is obtained.

An experimental system with collinear mixed-frequency ultrasound has been developed. The collected experimental data are analyzed to obtain the mixed-frequency nonlinear factors of the fatigue damage growth under the rising fatigue cycles. The relationship between the sum frequency nonlinearity coefficients and the relative parameters of the mixed ultrasonic wave nonlinearity is established. The model for predicting the fatigue crack growth of the metal specimens under the fatigue damage of the collinear mixed-frequency ultrasound has been established. Based on the average error analysis of crack depth prediction of difference frequency, sum frequency nonlinear coefficient, and mixing nonlinear relative coefficient, it shows that the prognosis model with the mixed-frequency nonlinear relative parameters is fully enough to characterize the dependence relationship between the fatigue damage and the mixed-frequency nonlinear factors.

Author Contributions: Project administration, H.C.; investigation, S.L. All authors have read and agreed to the published version of the manuscript.

Funding: This work was supported by the National Natural Science Foundation of China (Grant 51775390).

Institutional Review Board Statement: Not applicable.

Informed Consent Statement: Not applicable.

Data Availability Statement: Not applicable.

Conflicts of Interest: The authors declare no conflict of interest.

References

1. Chen, H.; Fan, D.; Huang, J.; Huang, W.; Zhang, G.; Huang, L. Finite element analysis model on ultrasonic phased array technique for material defect time of flight diffraction detection. *Sci. Adv. Mater.* **2020**, *12*, 665–675. [CrossRef]
2. Li, Y.J.; Chang, Q.C. Complex data study on mechanical fault diagnosing. *J. Intell. Fuzzy Syst.* **2018**, *34*, 1169–1176.
3. Chen, H.; Huang, W.; Huang, J.; Cao, C.; Yang, L.; He, Y.; Zeng, L. Multi-fault condition monitoring of slurry pump with principle component analysis and sequential hypothesis test. *Int. J. Pattern Recognit. Artif. Intell.* **2020**, *34*, 2059019. [CrossRef]
4. Chen, H.; Fan, D.L.; Fang, L.; Huang, W.; Huang, J.; Cao, C.; Yang, L.; He, Y.; Zeng, L. Particle swarm optimization algorithm with mutation operator for particle filter noise reduction in mechanical fault diagnosis. *Int. J. Pattern Recognit. Artif. Intell.* **2020**, *34*, 2058012. [CrossRef]
5. Chen, H.; Huang, L.; Yang, L.; Chen, Y.; Huang, J. Model-based method with nonlinear ultrasonic system identification for mechanical structural health assessment. *Trans. Emerg. Telecommun. Technol.* **2020**, *31*, e3955. [CrossRef]
6. Jones, G.L.; Kobett, D.R. Interaction of Elastic Waves in an Isotropic Solid. *J. Acoust. Soc. Am.* **1963**, *35*, 5–10. [CrossRef]
7. Kalayanasundaram, N. Nonlinear mode coupling of surface acoustic waves on an isotropic solid. *Int. J. Eng. Sci.* **1981**, *19*, 435–441. [CrossRef]
8. Kalyanasundaram, N. Nonlinear mixing of surface acoustie waves propagating in opposite directions. *J. Acoust. Soc. Am.* **1998**, *73*, 1956–1965. [CrossRef]
9. Walker, S.V.; Kim, J.Y.; Qu, J.; Jacobs, L.J. Fatigue damage evaluation in A36 steel using nonlinear Rayleigh surface waves. *NDT E Int.* **2012**, *48*, 10–15. [CrossRef]
10. Lim, H.J.; Sohn, H. Fatigue crack detection using structural nonlinearity reflected on linear ultrasonic features. *J. Appl. Phys.* **2015**, *118*, 244902. [CrossRef]
11. Chen, H.; Zhang, G.; Fan, D.; Fang, L.; Huang, L. Nonlinear Lamb Wave Analysis for Microdefect Identification in Mechanical Structural Health Assessment. *Measurement* **2020**, *164*, 108026. [CrossRef]
12. Jiao, J.; Sun, J.; Li, N.; Song, G.; Wu, B.; He, C. Micro-crack detection using a collinear wave mixing technique. *NDT E Int.* **2014**, *62*, 122–129. [CrossRef]
13. Chen, Z.; Tang, G.; Zhao, Y.; Jacobs, L.J.; Qu, J. Mixing of collinear plane wave pulses in elastic solids with quadratic nonlinearity. *J. Acoust. Soc. Am.* **2014**, *136*, 2389–2404. [CrossRef] [PubMed]
14. Zhang, F.; Li, C.; Tie, Y.; Yin, Z. Experimental study on fatigue damage detection based on nonlinear ultrasonic. *FRP Compos.* **2019**, *4*, 12–16.
15. Zheng, M.F. Numerical Simulation and Experimental Study of Pipeline Guided Wave Detection Technology. Master's Thesis, Nanchang University of Aeronautics, Nanchang, China, 2012.
16. Miao, Z.; Xiaochuan, Y.; Minggang, L. *ABAQUS-Based Finite Element Analysis and Applications*; Tsinghua University Press: Beijing, China, 2007.
17. Shi, Y.; Zhou, Y. *ABAQUS Finite Element Analysis Examples in Detail*; Machinery Industry Press: Beijing, China, 2013.
18. Wang, Z.; Hu, W.; Hu, L. *Session Service Criterion and the Theory and Application of Plastic Stress-Strain Relationship*; Higher Education Press: Beijing, China, 2014.
19. Qin, F.; Wu, B. *Fundamentals of Elasticity and Plasticity Theory*; Beijing Science Press: Beijing, China, 2011.
20. Zhao, J.; Qian, Z.; Xu, H.; Shuang, Z.; Zhang, R.; Yin, W. CFRP nondestructive flaw detection system based on electromagnetic detection technology. *Electron. Technol.* **2018**, *47*, 104–107.
21. Rosi, G.; Giorgio, I.; Eremeyev, V.A. Propagation of linear compression waves through plane interfacial layers and mass adsorption in second gradient fluids. *ZAMM-J. Appl. Math. Mech./Z. Angew. Math. Mech.* **2013**, *93*, 914–927. [CrossRef]
22. Placidi, L.; Anil, M.; Emilio, B. Simulation results for damage with evolving microstructure and growing strain gradient moduli. *Cotinuum Mech. Thermodyn.* **2019**, *31*, 1143–1163. [CrossRef]
23. Dell'Isola, F.; Madeo, A.; Placidi, L. Linear plane wave propagation and normal transmission and reflection at discontinuity surfaces in second gradient 3D continua. *ZAMM-J. Appl. Math. Mech./Z. Angew. Math. Mech.* **2012**, *92*, 52–71. [CrossRef]
24. Kim, J.-Y.; Qu, J.; Jacobs, L.J.; Littles, J.W.; Savage, M.F. Acoustic Nonlinearity Parameter Due to Microplasticity. *J. Nondestruct. Eval.* **2006**, *25*, 29–37. [CrossRef]